Journal Name

RSCPublishing

ARTICLE

Ni_2P enhances the activity and durability of Pt anode catalyst in direct methanol fuel cell

Cite this: DOI: 10.1039/x0xx00000x

Jinfa Chang[a]†, Ligang Feng[b]†, Changpeng Liu[a], Wei Xing[a*] and Xile Hu[b*]

Received 00th January 2012,
Accepted 00th January 2012

DOI: 10.1039/x0xx00000x

www.rsc.org/

Pt is the state-of-the-art anode catalyst in direct methanol fuel cells. Here we report that Ni_2P promotes the activity and stability of Pt in electrochemical methanol oxidation. Nanoparticles of Ni_2P and Pt were co-deposited on a carbon support and their activity in electrochemical methanol oxidation was measured by cyclic voltammetry. Among all Pt-Ni_2P/C catalysts, the sample with a 30 wt% loading of Ni_2P exhibits the highest electrochemical surface area and activity. The activity of Pt-Ni_2P/C-30% catalyst is significantly higher than Pt/C, Ni-promoted Pt/C, and P-promoted Pt/C catalysts, revealed by cyclic voltammetry, chronoamperometry, and electrochemical impedance spectroscopy. Accordingly to X-ray photoelectron spectroscopy, there is a partial electron transfer from Ni_2P to Pt, which might be an origin of the enhanced catalytic activity of the Pt/Ni_2P bimetallic catalyst. The Pt-Ni_2P/C-30% was integrated into a direct methanol fuel cell; this fuel cell exhibits a maximum power density of 65 mW/cm^2, more than twice of that of an analogues fuel cell using Pt/C as anode catalyst. The Pt-Ni_2P/C-30%-integrated direct methanol fuel cell has also the highest discharge stability among a series of fuel cells with different Pt-based anode catalysts.

Introduction

Direct methanol fuel cells (DMFCs) are considered as promising future power conversion devices for stationary and mobile applications[1-3]. However, the cost of the precious metals employed as catalysts and the low life-time of these catalysts due to poisoning by surface-adsorbed intermediate spices such as CO and CHO are key factors that prevent the commercialization of DMFCs[4-7]. State-of-the-art DMFCs employ Pt as the anode catalyst for the oxidation of methanol. Improving the activity and stability of Pt can lead to a lower loading of Pt which is beneficial for eventual commercialization. The introduction of an earth-abundant and non-precious co-catalyst is an effective approach to improve the catalytic activity and durability as well as to lower the cost of Pt-based catalysts[3, 6, 8, 9]. Several metal oxides such as WO_x[10, 11], MoO_x[12, 13], CeO_2[14, 15], and SnO_2[16], as well as main group elements such as P[17] and N,[18] have been used to promote Pt in methanol oxidation. Unfortunately the instability of the promoters under the operating conditions resulted in a rapid decay of the catalytic performance.

Recently, we found that Ni_2P was an effective co-catalyst for Pd-catalyzed formic acid oxidation[19]. The Pd-Ni_2P/C anode system showed remarkable catalytic activity and stability. Moreover, the promotional effect of Ni_2P is much larger than P or Ni alone. It was reported Ni and P enhanced the activity and durability of Pt anode catalyst for methanol oxidation[20-23]. Inspired by these previous findings, we examined the possible promotion of Pt by Ni_2P in methanol oxidation. To our delight, the promotional effect of Ni_2P on Pt was remarkable. Here we report the preparation, characterization, and catalytic property of the Pt-Ni_2P/C anode catalyst system.

Results and discussion

The synthesis of Ni_2P, Ni_2P/C, and Pt-Ni_2P/C is described in the experimental section. The Ni_2P/C materials are characterized by Raman spectroscopy (Fig. S1) and XRD (Fig. S2). The data are in agreement with those previously reported[19]. In the XRD pattern of Pt-Ni_2P/C, the peaks from Ni_2P are invisible (Fig. S3), probably because they were buried under the strong and broad peaks of Pt. Similar observation was earlier made on Pd-Ni_2P/C samples[19]. The presence of Ni_2P in Pt-Ni_2P/C was confirmed by Energy Dispersive X-ray Spectroscopy (EDX) (Fig. S4a) and the element distribution maps (Fig. S4c-i). The width of the (220) diffraction peak of Pt was used to calculate the size of Pt particles, which indicated an average size of 2.5 nm for Pt in all Pt-Ni_2P/C samples.

Typical transmission electron microscopy (TEM) images of Ni_2P/C and Pt-Ni_2P/C (30 wt.% of Ni_2P on C) are shown in Figure 1. The Ni_2P nanoparticles can be identified by a finger lattice of 0.221 nm corresponding to its (111) lattice (Figure 1a).

After deposition of Pt on Ni_2P/C, the Pt nanoparticles were uniformly distributed over the whole surface (Figure 1b). Many Pt nanoparticles resided close to Ni_2P nanoparticles (Figure 1c). Finger lattices of Ni_2P and Pt can be both observed (Figure 1c). The average size of Pt is about 2.4 nm (Figure 1b and d), consistent with the value obtained from XRD measurement. The size distribution of Pt is relatively uniform. The TEM and HRTEM images of Pt-Ni_2P/C samples with other loadings of Ni_2P are shown in Figure S5). The particle sizes in all samples are similar, and are consistent with the values calculated by applying the Scherrer equation to the diffraction pattern (Table S 1).

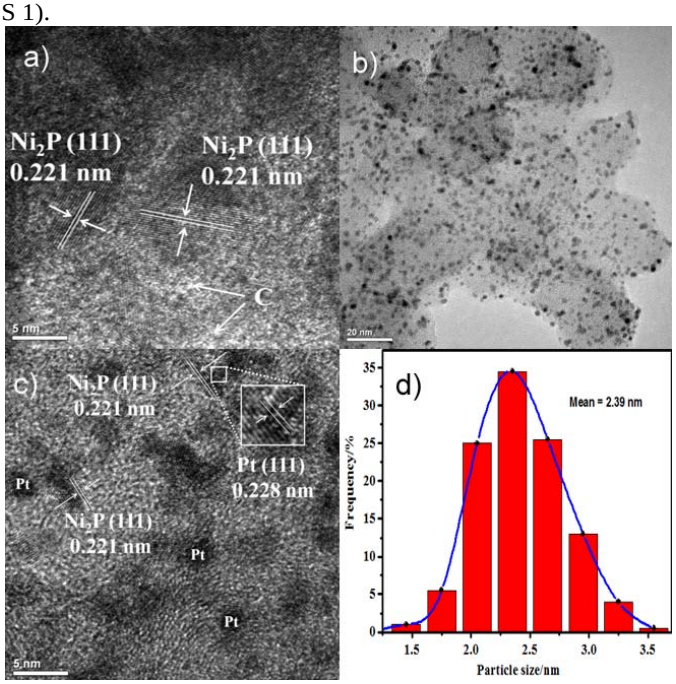

Figure 1(a) HRTEM image of a Ni_2P/C sample. (b) TEM and (C) HRTEM images of a Pt-Ni_2P/C-30% sample. (d) Particle size distribution of Pt in Pt-Ni_2P/C-30%.

For comparison, Ni-promoted Pt (Pt-Ni/C), P-promoted Pt (Pt-P/C), commercial Pt/C-JM (Johnson Matthey), and home-made Pt/C-H catalysts were also employed in the electrochemical studies. All Pt-Ni_2P/C samples and the Pt-based reference catalysts exhibit typical electrochemical behaviours of Pt in 0.5 M H_2SO_4 (Fig. S6). The electrochemical surface area (ECSA) can be estimated from either hydrogen desorption peaks or CO stripping experiments (Fig. S7). The Pt-Ni_2P/C-30% sample has the largest ECSA even though the loading of Pt is the same in all samples (Table S2). The ECSAs obtained from CO-stripping experiments were used to calculate the specific activity for all catalysts. The peak potential of CO absorption is commonly used as a parameter to compare the anti-poisoning property of methanol oxidation catalysts[24, 25]. The Pt-Ni_2P/C-30% catalyst has the lowest peak potential (Table S2), indicating that this material has the best anti-poisoning property.

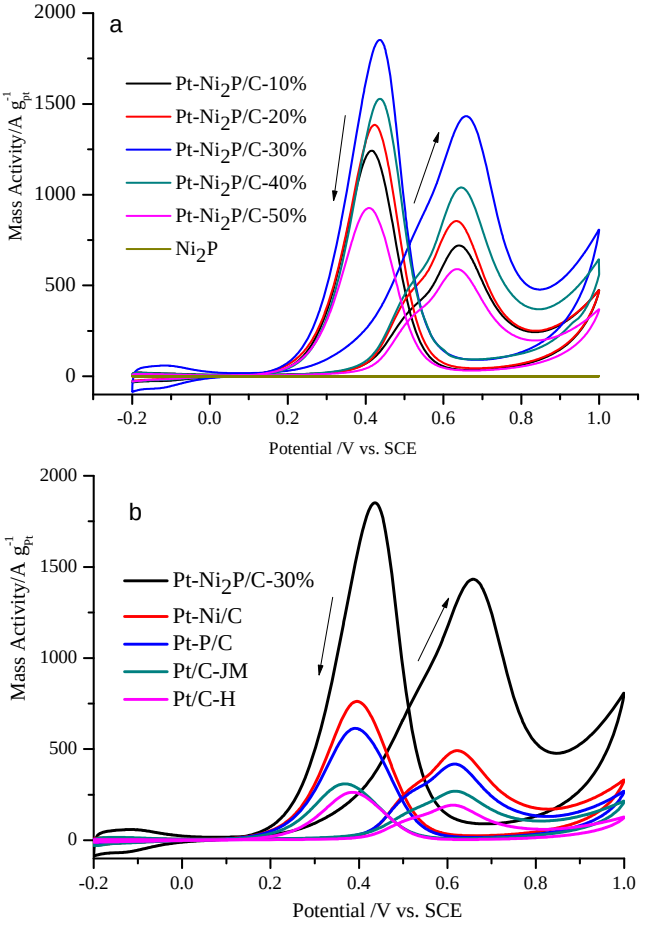

Figure 2. (A) Cyclic voltammograms of Pt-Ni_2P/C catalysts with various loadings of Ni_2P in H_2SO_4 solution (0.5 M) containing CH_3OH (1 M). (b) Cyclic voltammograms of Pt-Ni_2P/C-30%, Pt-Ni/C, Pt-P/C, Pt/C-JM and Pt/C-H catalysts in H_2SO_4 solution (0.5 M) containing CH_3OH (1M).

The activity of all catalyst in electrochemical methanol oxidation was first measured by cyclic voltammetry (CV). Figure 2 shows the mass activity, Fig. S8 shows the specific activity, and Table S3 compares peak current in the positive scan. Ni_2P alone has no catalytic activity; however, it has a strong influence on the activity of Pt. The optimized loading of Ni_2P is 30 wt% on carbon (Figure 2a). Judging from the peak currents, the Pt-Ni_2P/C-30% catalyst is the best catalyst compared with other Pt/C catalysts; it is about 7 times as active as the Pt/C-H catalyst, 5 times as active as the Pt/C-JM catalyst, and 3 times as active as the Pt-Ni/C and Pt-P/C catalysts. While N and Ni seem to promote the activity of Pt, the promotion is much less compared with that by Ni_2P (Figure 2b). A recent study showed that porous Pt-Ni-P ternary composite nanotube arrays are a good anode catalyst for methanol oxidation.[26] A specific peak current of 3.85 mA/cm^{-2} was obtained using that catalyst, which is still lower than the peak current of the Pt-Ni_2P/C-30% catalyst reported here (4.05 mA/cm^{-2}). The synthetic procedure for the Pt-Ni_2P/C catalyst is also much simpler than that of the Pt-Ni-P composite nanotubes. The

superior activity of Pt-Ni_2P/C-30% catalyst was also confirmed by chronoamperometric (CA) measurements at 0.6 V vs. SCE (Fig. S9), and furthermore, the activity of Pt-Ni_2P/C-30% compares favourably with other recently reported catalysts (Table S4).

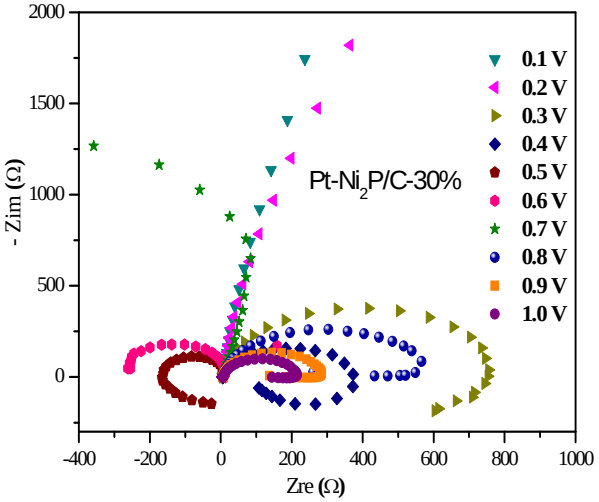

Figure 3. Nyquist plots for the Pt-Ni_2P/C-30% catalyst in electrochemical methanol oxidation at different potentials.

Electrochemical Impedance Spectroscopy (EIS) was used to investigate the kinetics of methanol oxidation at different potentials.[27] The Nyquist plots for Pt-Ni_2P/C-30% are shown in Figure 3; those of other Pt-based catalysts are shown in Figure S10. In agreement with the CV data, no methanol oxidation occurred below 0.3 V, so only straight lines were observed in the EIS spectra below 0.3 V. At 0.30-0.4 V, a "pseudoinductive" behavior was observed, in which a positive loop at higher frequencies was accompanied by a low frequency loop in the fourth quadrant. This is a common behavior for Pt-catalyzed methanol oxidation, and is an indication that methanol is first dehydrogenated to form adsorbed CO species which is then oxidatively removed[28, 29]. At 0.5-0.7 V the shapes of the Nyquist plots changes dramatically; the plots are located in the second and third quadrants; in the literature, this is considered as a sign that the rate-determining step of methanol oxidation changes from methanol dehydrogenation to oxidative removal of CO_{ads} by OH_{ads}. A further increase of potential actually decreases the rate of methanol oxidation, as the adsorption of OH is too strong at high potentials and it starts to inhibit Pt-catalyzed methanol oxidation. This is consistent with the peak potential of 0.65 V observed by CV (Figure 2). In the EIS spectra, this decrease of reaction rate is reflected in a new "pseudoinductive" behavior at > 0.8 V. With a further increase of potential beyond 0.8 V, the diameter of the semicircles decreases due to the oxidation of the Pt active sites at high potentials. This is consistent with the current increase at 0.9-1.0 V in the CV.

The data from EIS can also be used to compare the activity of various methanol oxidation catalysts. The Niquist plots at 0.5 V of representative catalysts are shown in Figure 4. The diameter of the EIS semicircle or arc correlates with charge transfer resistance. The smaller the diameter, the lower the resistance, and the higher the methanol oxidation rate. Accordingly to Figure 4, the semicircle from the Pt-Ni_2P/C-30% catalyst has the smallest diameter, and hence this catalyst has the highest activity in methanol oxidation.

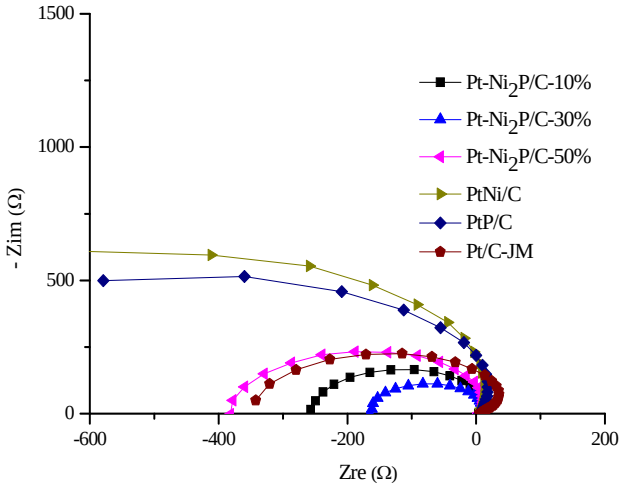

Figure 4. Nyquist plots of various Pt and promoted Pt catalysts for methanol oxidation at 0.5 V.

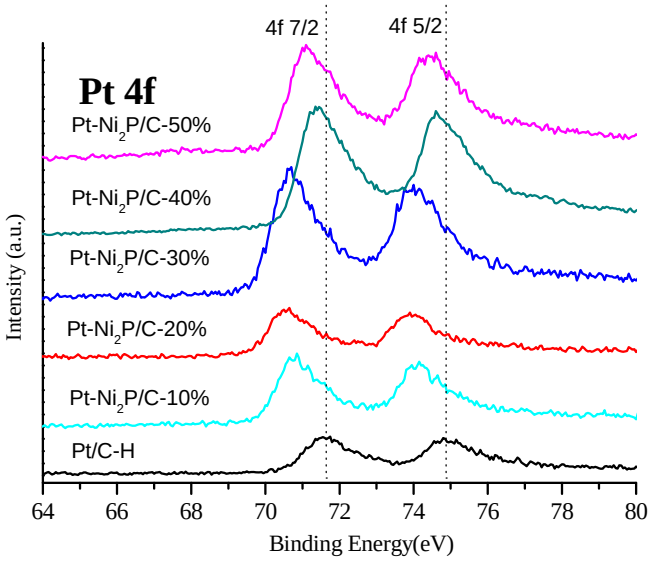

Figure 5. XPS spectra of the Pt 4f region for Pt/C-H and Pt-Ni_2P/C catalysts.

X-ray photoelectron spectroscopy (XPS) was used to probe the electronic interaction of Ni_2P and Pt in thePt-Ni_2P/C catalyst. Figure 5 shows the Pt 4f XPS spectra. The Pt/C-H catalyst exhibits two peaks at 71.6 and 74.8 eV. These Pt 4f peaks are significantly shifted to lower binding energies. In the optimized Pt-Ni_2P/C-30% catalyst, the shift was about 1.0 eV. An even higher loading of Ni_2P, however, resulted in a smaller shift. This is probably due to aggregation of the nanoparticles at high loadings which is detrimental for an optimized Ni_2P-Pt interaction. This large shift in the binding energies of Pt 4f

peaks upon promotion by Ni_2P indicates a partial electron transfer from Ni_2P to Pt, which may be one factor for the enhanced catalytic activity in the Pt-Ni_2P/C catalyst. This type of interaction may change the electronic structure and density of state of metal catalysts and weaken the binding energy of strongly adsorbed and poisonous intermediates [30-32]. In addition to the electronic effect, the presence of Ni_2P might also activate water, producing -OH_{ads} to oxidize CO and other poisoning intermediates adsorbed at adjacent Pt sites through the so-called bi-functional mechanism[33, 34].

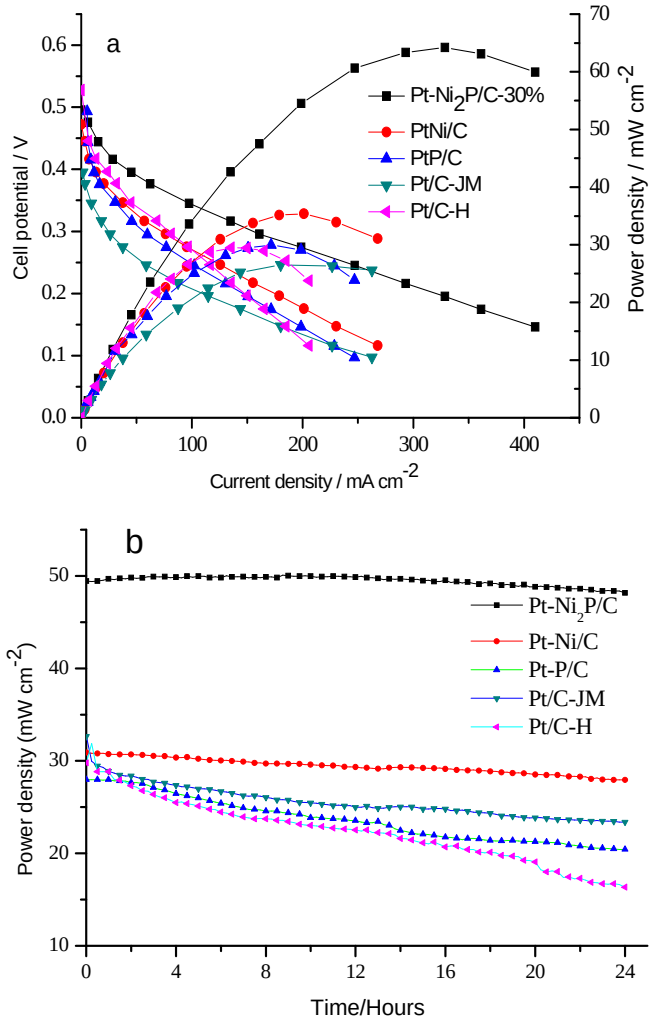

Figure 6. (a) Steady-state polarization and power-density curves for fuel cells employing for Pt-Ni_2P/C-30%, Pt-Ni/C, Pt-P/C, Pt/C-JM and Pt/C-H as anode catalysts. (b)The discharge curves at 0.3V for for fuel cells employing for Pt-Ni_2P/C-30%, Pt-Ni/C, Pt-P/C, Pt/C-JM and Pt/C-H as anode catalysts. Conditions: 1 M methanol at 60 °C. The flowing rate of methanol was 20 mL min^{-1} and the flowing rate of O_2 was 200 mL min^{-1}.

To demonstrate the potential of the Pt-Ni_2P/C anode catalysts in DMFCs, a sample of Pt-Ni_2P/C-30% was integrated onto the anode of a homemade DMFC. Figure 6a shows the steady-stead polarization and power density curves of this fuel cell, together with analogous fuel cells with reference catalysts. The fuel cell with the Pt-Ni_2P/C-30% anode catalyst exhibits a higher current density than all other fuel cells at the same potential. As a result, this fuel cell has the highest power density as well, with a maximum power density of 65 mW cm^{-2}. According to Figure 6 (a), its power density is about twice of those of analogous cells employing state-of-the-art Pt catalysts. Figure 6b shows the discharge curves of all these fuel cells at 0.3 V. The cell with the Pt-Ni_2P/C-30% anode catalyst not only has the highest power density, but also the highest stability: the power density remains stable during 24h.

Conclusions

Nanoparticles of Ni_2P and Pt were co-deposited onto a carbon support and the resulting Pt-Ni_2P/C hybrid catalyst showed excellent activity in electrochemical methanol oxidation. The Ni_2P nanoparticles significantly promote the activity and stability of Pt in methanol oxidation. The promotion is at least partially due to a strong electronic interaction between Ni_2P and Pt, resulting in a partial electron transfer from Ni_2P to Pt. A direct methanol fuel cell employing the optimized Pt-Ni_2P/C anode catalyst has a power density that is twice of those of analogous fuel cells employing state-of-the-art Pt-based catalysts. The discovery of inexpensive and earth-abundant Ni_2P as a promoter in Pt-catalyzed methanol oxidation is a significant advance in the development of affordable direct methanol fuel cells.

Experimental

Synthesis of Ni_2P nanoparticles and Ni_2P/C hybrid

The synthesis is described in an earlier paper.[19] In brief, a solid mixture of 0.66 g $NaH_2PO_2 \cdot H_2O$ and 0.3 g $NiCl_2 \cdot 6H_2O$ was mechanically mixed in a quartz boat at room temperature. The precursor was heated to 250 °C and kept for 1 h in a flowing 30 mL min^{-1} N_2. Following cooling to room temperature in a continuous N_2 flow, the unsupported Ni_2P nanoparticles were passivated in a 1.0 mol% O_2/N_2 mixture at 20 mL min^{-1} for 3 h. Carbon-supported Ni_2P was prepared as follows. 0.218 g Vulcan XC-72 was incipiently impregnated with an aqueous solution of 0.3g $NiCl_2 \cdot 6H_2O$ and then dried at 120 °C for 3h. The next steps are similar to those employed to prepare unsupported Ni_2P particles. The loading of Ni_2P was varied from 10% to 50% with respect to C.

Synthesis of Pt-Ni_2P/C

Pt-Ni_2P/C composites with 20 wt% Pt were prepared by a microwave-assisted ethylene glycol reduction process. 80 mg of Ni_2P/C was ultrasonically dispersed in 50 ml of ethylene glycol to form a uniform suspension. Under stirring, a certain amount of $H_2PtCl_6 \cdot 6H_2O$ solution containing 20 mg Pt was added to the above suspension, and the pH of the suspension was adjusted to about 11.0 with a 1.0 M NaOH solution. The resulting suspension was placed in the middle of a microwave oven

operating at 700 W for 90 s and was then cooled to room temperature naturally. The suspension was finally filtered, washed and dried overnight at 80 °C in a vacuum oven to obtain the Pt-Ni_2P/C catalyst.

The platinum catalyst supported on XC-72 (denoted as Pt/C-H) was prepared by the same method. Carbon supported PtNi catalyst (denoted as Pt-Ni/C) was synthesized using a similar method except that both a$H_2PtCl_6{\cdot}6H_2O$ solution containing 20 mg Pt) and a $NiCl_2{\cdot}6H_2O$ solution containing 20 mg Ni were added to the initial suspension. Carbon supported PtP catalyst (denoted as Pt-P/C) was synthesized using a similar method except that a $H_2PtCl_6{\cdot}6H_2O$ solution containing 20 mg Pt and $NaH_2PO_2{\cdot}H_2O$ (the mole ratios of Pt : $H_2PO_2^-$ = 1:60) was added to the initial suspension. Commercial state-of-the-art 20 wt% Pt/C catalyst (Johnson Matthey Company, HiSPECTM 3000, denoted as Pt/C-JM) was used as a reference. Other experiments details are described in the supporting information.

Acknowledgements

The work in CAS is supported by the National Basic Research Program of China (973 Program, 2012CB215500, 2012CB932800), the National High Technology Research and Development Program of China (863 Program, 2012AA053401), the Recruitment Program of Foreign Experts (WQ20122200077), the National Natural Science Foundation of China (20933004, 21073180) and the Strategic priority research program of CAS (XDA0903104). The work at EPFL is supported by a grant from the Competence Center for Energy and Mobility (CCEM) in the framework of the Hytech project.

Notes and references

[a]State Key Laboratory of Electroanalytical Chemistry, Laboratory of Advanced Power Sources, Changchun Institute of Applied Chemistry, Chinese Academy of Sciences, Changchun 130022 (P.R. China)
Fax: 86-431-85685653, E-mail: xingwei@ciac.jl.cn
[b]Laboratory of Inorganic Synthesis and Catalysis, Institute of Chemical Sciences and Engineering, Ecole Polytechnique Fédérale de Lausanne (EPFL), ISIC-LSCI, BCH 3305, Lausanne 1015, Switzerland
Fax: (+) 49 21 693 9305, E-mail: xile.hu@epfl.ch
† These authors contributed equally to this work.

Electronic Supplementary Information (ESI) available: experimental details, additional figures and tables. See DOI: 10.1039/b000000x/

1. E. Reddington, *Science*, 1998, **280**, 1735-1737.
2. C. Koenigsmann and S. S. Wong, *Energy Environ. Sci.*, 2011, **4**, 1161.
3. Z.-Z. Jiang, Z.-B. Wang, Y.-Y. Chu, D.-M. Gu and G.-P. Yin, *Energy Environ. Sci.*, 2011, **4**, 2558.
4. F. Jaouen, E. Proietti, M. Lefevre, R. Chenitz, J.-P. Dodelet, G. Wu, H. T. Chung, C. M. Johnston, P. Zelenay and J.-B. Ju, *Energy Environ. Sci.* , 2011, **4**, 114-130.
5. X. Zhao, M. Yin, L. Ma, L. Liang, C. Liu, J. Liao, T. Lu and W. Xing, *Energy Environ. Sci.*, 2011, **4**, 2736–2753.
6. R. Ganesan and J. S. Lee, *Angew. Chem. Int. Ed.*, 2005, **44**, 6557-6560.
7. A. Chen and P. Holt-Hindle, *Chem. Rev.*, 2010, **110**, 3767–3804.
8. V. T. Thanh Ho, K. C. Pillai, H.-L. Chou, C.-J. Pan, J. Rick, W.-N. Su, B.-J. Hwang, J.-F. Lee, H.-S. Sheu and W.-T. Chuang, *Energy Environ. Sci.* , 2011, **4**, 4194.
9. L. Feng, Q. Lv, X. Sun, S. Yao, C. Liu and W. Xing, *J. Electroanal. Chem.*, 2012, **664**, 14-19.
10. Z. Cui, L. Feng, C. Liu and W. Xing, *J Power Sources*, 2011, **196**, 2621-2626.
11. P. Trogadas and V. Ramani, *J. Electrochem. Soc.*, 2008, **155**, B696-B703.
12. L. Feng, Q. Lv, X. Sun, S. Yao, C. Liu and W. Xing, *J. Electroanal. Chem.*, 2012, **664**, 14-19.
13. Z. M. Cui, S. P. Jiang and C. M. Li, *Chem. Commun.*, 2011, **47**, 8418-8420.
14. J. W. Guo, T. S. Zhao, J. Prabhuram, R. Chen and C. W. Wong, *J. Power Sources*, 2006, **156**, 345-354.
15. D.-M. Gu, Y.-Y. Chu, Z.-B. Wang, Z.-Z. Jiang, G.-P. Yin and Y. Liu, *Appl. Catal. B: Environ.*, 2011, **102**, 9-18.
16. S. Yang, C. Zhao, C. Ge, X. Dong, X. Liu, Y. Liu, Y. Fang, H. Wang and Z. Li, *J. Mater. Chem.*, 2012, **22**, 7104.
17. J. P. Paraknowitsch and A. Thomas, *Energy Environ. Sci.*, 2013, **6**, 2839.
18. X. H. Li and M. Antonietti, *Chemical Society reviews*, 2013, **42**, 6593-6604.
19. J. Chang, L. Feng, C. Liu, W. Xing and X. Hu, *Angew. Chem. Int. Ed.*, 2014, **53**, 122-126.
20. B. M. Leonard, Q. Zhou, D. Wu and F. J. DiSalvo, *Chem. Mater.*, 2011, **23**, 1136-1146.
21. T. C. Deivaraj, W. X. Chen and J. Y. Lee, *J. Mater. Chem.*, 2003, **13**, 2555-2560.
22. M.-L. Lin, M.-Y. Lo and C.-Y. Mou, *Catal. Today*, 2011, **160**, 109-115.
23. H. Daimon and Y. Kurobe, *Catal. Today*, 2006, **111**, 182-187.
24. X. Cui, L. Guo, F. Cui, Q. He and J. Shi, *J. Phys. Chem. C*, 2009, **113**, 4134-4138.
25. L. Feng, X. Zhao, J. Yang, W. Xing and C. Liu, *Catal. Commun.*, 2011, **14**, 10-14.
26. L. X. Ding, A. L. Wang, G. R. Li, Z. Q. Liu, W. X. Zhao, C. Y. Su and Y. X. Tong, *J. Am. Chem. Soc.*, 2012, **134**, 5730-5733.
27. B. Ma, J. C. Bai and L. F. Dong, *J. Solid State Electrochem.*, 2013, **17**, 2783-2788.
28. G. Wu, L. Li and B. Q. Xu, *Electrochim. Acta*, 2004, **50**, 1-10.
29. É. C. G. Rufino and P. Olivi, *Int. J. Hydrogen Energy*, 2010, **35**, 13298-13308.
30. Y. K. Zhou, R. Pasquarelli, T. Holme, J. Berry, D. Ginley and R. O'Hayre, *J. Mater. Chem.*, 2009, **19**, 7830-7838.
31. R. O'Hayre, S. Pylypenko, A. Queen, T. S. Olson, A. Dameron, K. O'Neill, K. C. Neyerlin, B. Pivovar, H. N. Dinh, D. S. Ginley and T. Gennett, *J. Phys. Chem. C*, 2011, **115**, 13676-13684.
32. S. Pylypenko, A. Queen, T. S. Olson, A. Dameron, K. O'Neill, K. C. Neyerlin, B. Pivovar, H. N. Dinh, D. S. Ginley, T. Gennett and R. O'Hayre, *J. Phys. Chem. C*, 2011, **115**, 13667-13675.
33. H. J. Kim, D. Y. Kim, H. Han and Y. G. Shul, *J. Power Sources*, 2006, **159**, 484-490.
34. C. Rice, S. Ha, R. I. Masel and A. Wieckowski, *J. Power Sources*, 2003, **115**, 229-235.

TOC figure